Scripta Materialia 171 (2019) 52–56

Contents lists available at ScienceDirect

Scripta Materialia

journal homepage: www.elsevier.com/locate/scriptamat

Mechanical properties of supersonic-impacted Al6061 powder particles

Tyler J. Flanagan [a,*], Benjamin A. Bedard [a], Avinash M. Dongare [a], Harold D. Brody [a], Aaron Nardi [b], Victor K. Champagne Jr [b], Mark Aindow [a], Seok-Woo Lee [a]

[a] Department of Materials Science and Engineering, Institute of Materials Science, University of Connecticut, 97 North Eagleville Road, Unit 3136, Storrs, CT 06269-3136, USA
[b] U.S. Army Research Laboratory, Weapons and Materials Research Directorate, Aberdeen Proving Ground, Aberdeen, MD, 21005, USA

ARTICLE INFO

Article history:
Received 11 May 2019
Received in revised form 13 June 2019
Accepted 16 June 2019
Available online 27 June 2019

Keywords:
High-speed deformation
Severe plastic deformation
Tension test
Dislocation
Aluminum alloys

ABSTRACT

The cold spray process utilizes a high-pressure gas jet to accelerate metallic particles to supersonic velocities, causing bonding to the substrate upon impact. The mechanical characterization of impacted particles is of great interest as their mechanical properties are strongly related to those of bulk cold-sprayed coatings. Here, in-situ micro-compression and tension results are presented from impacts in single-pass cold spray trials of as-atomized and heat-treated Al6061 powders. The effects of powder microstructure on the yield strength and ductility of individual impacts are discussed. Such observations contribute to a more fundamental understanding of the mechanical behavior of impacted metallic materials.

The cold spray process is a solid-state additive manufacturing technique in which micron-sized metallic particles are accelerated to supersonic velocities via a high-pressure gas jet [1]. Upon impact with a suitable substrate surface, the particles undergo severe plastic deformation and, above the material's critical impact velocity, undergo adiabatic heating and hydrodynamic plasticity resulting in metallurgical bonding [1–9]. The cold-spray process has several advantages when compared to traditional thermal spray techniques. By not exposing the powder particles to high temperatures, unfavorable reactions such as oxidation and other diffusion-controlled reactions are inhibited [10–12]. Additionally, the effects of the deposition on the substrate's microstructure and resultant properties are minimal, making cold spray an attractive approach for structural repair coatings [13–15].

The material properties of cold-spray coatings are usually strongly related to the initial microstructures and mechanical properties of the feedstock powder particles, primarily because the solid-state nature of the process and relatively low temperatures do not tend to substantively change the microstructures during deposition [16–20]. Microstructural features including grain structures, dislocation content, precipitation, and surface oxide films for individual powder particles affect their plastic flow behavior at the moment of supersonic impact; this controls the critical velocity and adhesion strength of the individual impacts, and eventually the mechanical properties of bulk cold-spray deposits [16–21]. In order to understand the macroscopic properties of cold-spray deposits in more detail, it is necessary to understand how the processes that occur during cold-spray impact affect both the microstructures and mechanical properties of individual powder particles.

The alloy Al6061 is of particular interest as a cold-spray deposition material due to its widespread use as a light-weight and high strength structural material and its relatively low critical impact velocity for cold-spray deposition [10,11]. Studies on the microstructures of powder particles and bulk-scale mechanical properties of bulk cold-sprayed Al6061 deposits have been extensive [22–26]. Research on the mechanical properties of the individual powder particles, however, is scarce. Due to the small sizes of the powder particles used (20–70 μm), it is extremely difficult to perform conventional uni-axial mechanical testing on these materials. Nano-indentation has been utilized to probe hardness and Young's modulus [22]. Due to the experimental challenges, uni-axial mechanical properties, such as yield strength and ductility, of individual powder particles before and after impact have not been studied previously. Recently, micropillar compression/tension techniques have been developed to study small-scale mechanical properties [23–26]. Focused-ion-beam milling (FIB) can produce micron-sized cylindrical micropillars and dog-bone specimens, which can be tested using advanced micromechanical testing systems.

In this study, we investigated the mechanical properties of individual Al6061 powder particles in different microstructural conditions, and impact splats from these powders, by using in-situ micropillar compression and tension testing. The objective of the investigation was to develop a more fundamental understanding of how the impact velocity and initial microstructure influence the mechanical properties of

* Corresponding author at: Department of Materials Science and Engineering, Institute of Materials Science, 97 North Eagleville Road, Unit 3136, Storrs, CT 06269-3136, USA.
E-mail address: tyler.flanagan@uconn.edu (T.J. Flanagan).

https://doi.org/10.1016/j.scriptamat.2019.06.024
1359-6462/

Al6061 powder particles before and after supersonic impact. Scanning transmission electron microscopy (STEM) was also used to observe the dislocation structure of the impacted splats, to help explain the effects of impact velocity on yield strength and ductility. The results obtained will help to develop a more fundamental understanding of the high strain rate deformation mechanisms occurring during the cold-spray process in Al6061 powder particles.

All experiments were performed using a single batch of commercial gas-atomized Al6061 powder obtained from Valimet, Inc. The powder was studied in three conditions: as-atomized, air-aged and homogenized. The air-aged batch was ramped to 230 °C in laboratory air, held at temperature for 75 min, removed from the furnace, and allowed to cool to room temperature. The homogenized batch was processed under argon by ramping to 400 °C, holding for 2 h, ramping to 530 °C, holding for 30 min, then cooling rapidly to room temperature. This homogenization was performed in a small welded retort which was filled partially with powder, heated in a box furnace, and then rapidly cooled by quenching and agitating in cool water. For each condition, low-coverage cold-spray trials were conducted using T6 Al6061 substrates and average impact velocities of 767 and 927 m/s. Nine different cases are considered in this study, comprising powder and splats with two different impact velocities for each of the three heat-treatment conditions. More detail on the heat treatment conditions and the microstructural characteristics of the samples are reported elsewhere [27].

In order to characterize the mechanical properties of the powder particles and their splats, cylindrical micropillars were fabricated for uniaxial compression tests and micron-sized dog-bone specimens for uniaxial tensile tests using a Helios Xe plasma FIB and a Helios NanoLab 460F1 Ga FIB (Thermo-Fisher, USA) (Fig. 1). The diameters of the micropillar specimens for the compression tests were about 5 μm and the thicknesses of the tensile specimens were about 3 μm. Further details of the micro-mechanical sample preparation and testing procedures are given in the online Supplementary Material. The micropillar sizes used in this study are large enough to exhibit only very weak size effects based on previous studies [27]. As such, size effects are not considered in this paper. Tensile testing could only be performed on the splats, because of difficulties in attaching the powder particles reliably. Micro-compression tests have been completed for all cases. It should be noted that for the cases of splat testing, the micro-mechanical test specimens included only the central region of the particle where the strain deformation is slightly lower than the particle periphery, but is relatively uniform. This allows for the study of the effect of high velocity impacts while avoiding strong gradients of microstructure and properties in our micropillar and micro-dogbone test specimens.

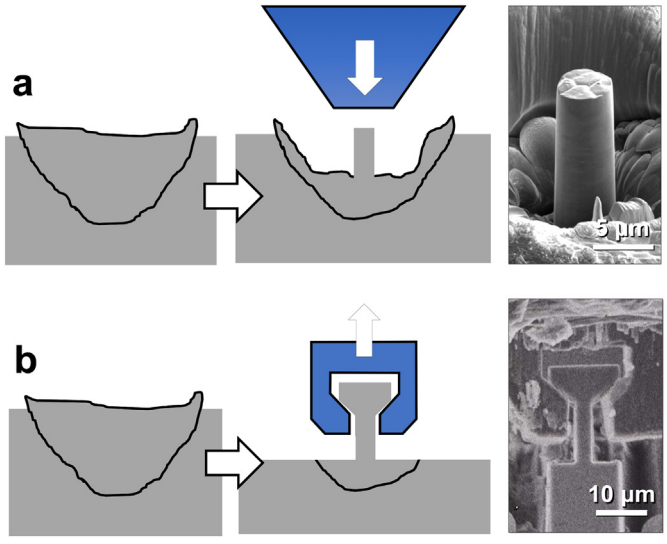

Fig. 1. Schematic diagrams and SEM micrographs showing the micromechanical testing procedures for: (a) micro-compression and (b) micro-tension tests.

In-situ micro-mechanical compression and tension testing were performed by using a NanoFlip™ system (KLA-Tencor, USA) mounted within a JEOL 6335F field-emission gun SEM (JEOL, Japan) (Fig. 1). The micro-pillars were tested at a nominal displacement rate of 10 nm/s, which corresponds to an approximate strain rate of $10^{-3}\,s^{-1}$. The dislocation structures in the splats were characterized by STEM using a Talos F200X (Thermo-Fisher, USA) operating at an accelerating voltage of 200 kV.

The progress of a typical micro-pillar compression test is shown in online Supplementary Movie 1 for the case of a 927 m/s splat from as-atomized powder. Examples of the compressive stress-strain curves obtained for each case are shown in Fig. 2(a). A flow stress of 0.05 plastic strain is used as a measure of the yielding behavior in all cases, as indicated by the arrows on the compressive stress-strain curves. This value is obtained by identifying the linear elastic portion of the curve, constructing a line parallel to this region, displacing the line by an increment of +0.05 strain, and finding the value of the stress where this line intersects the stress-strain curve.

For the powder particles, the as-atomized and air-aged samples showed similar deformation behavior with comparable values of the flow stress (190±8 MPa). For the homogenized powder particle case, however, there is an increase in flow stress to 229±4 MPa due to solid solution strengthening acting to impede dislocation motion [27]. The splat samples exhibited much higher values of the flow stress at 324 ± 13 MPa with surprisingly little effect of the impact velocity or heat-treatment condition on the mechanical behavior.

The corresponding tensile stress-strain curves are shown in Fig. 2(b). As noted above, these tensile tests were only completed successfully for the splats due to the adhesion issue. The splats produced from as-atomized and air-aged powders exhibited similar tensile stress-strain behavior for both impact velocities. The curves are characterized by rapid strain hardening resulting in low ductility (4–6%) elongation before failure (see also Supplementary Movies 2 and 3). The homogenized sample however showed significantly higher ductility (8–10%) (see also Supplementary Movie 4). The flow stress values obtained from the tensile samples (307 ± 32 MPa) are less than those from the compression tests (324 ± 13 MPa). This small difference is a result of the high offset strain used to measure the flow stress in the compression tests.

It is notable that the flow stress values are similar for all splat samples regardless of differences in the initial microstructure and impact velocity for compression and tension. The mechanical properties are closely related to the microstructure, implying that the relevant microstructural features are similar in all splats after supersonic impact. Supersonic impact certainly induces high strain rate and severe plastic deformation in Al6061 powder particles, leading to high dislocation densities. Aluminum has a high stacking fault energy, which results in compact dislocation cores. Under these circumstances, dislocation cross-slip can occur easily, and this could lead to dislocation annihilation that limits the maximum dislocation density. This dislocation saturation behavior is called dynamic recovery and is often observed in the stage III hardening in various FCC metals; the saturation phenomenon corresponds to the point when the dislocation multiplication rate becomes the same as the dislocation annihilation rate [28]. In this deformation regime, additional plastic deformation does not alter the overall dislocation structure. It would appear that the supersonic impact at a velocity of 767 m/s induces sufficient plastic deformation to generate the saturated dislocation structure, and so impacts at velocities higher than this could still produce similar microstructures and exhibit similar mechanical properties. The saturation of the dislocation structure due to dynamic recovery could be responsible for the weak effect of impact velocity on the flow stresses of the splats observed in this study.

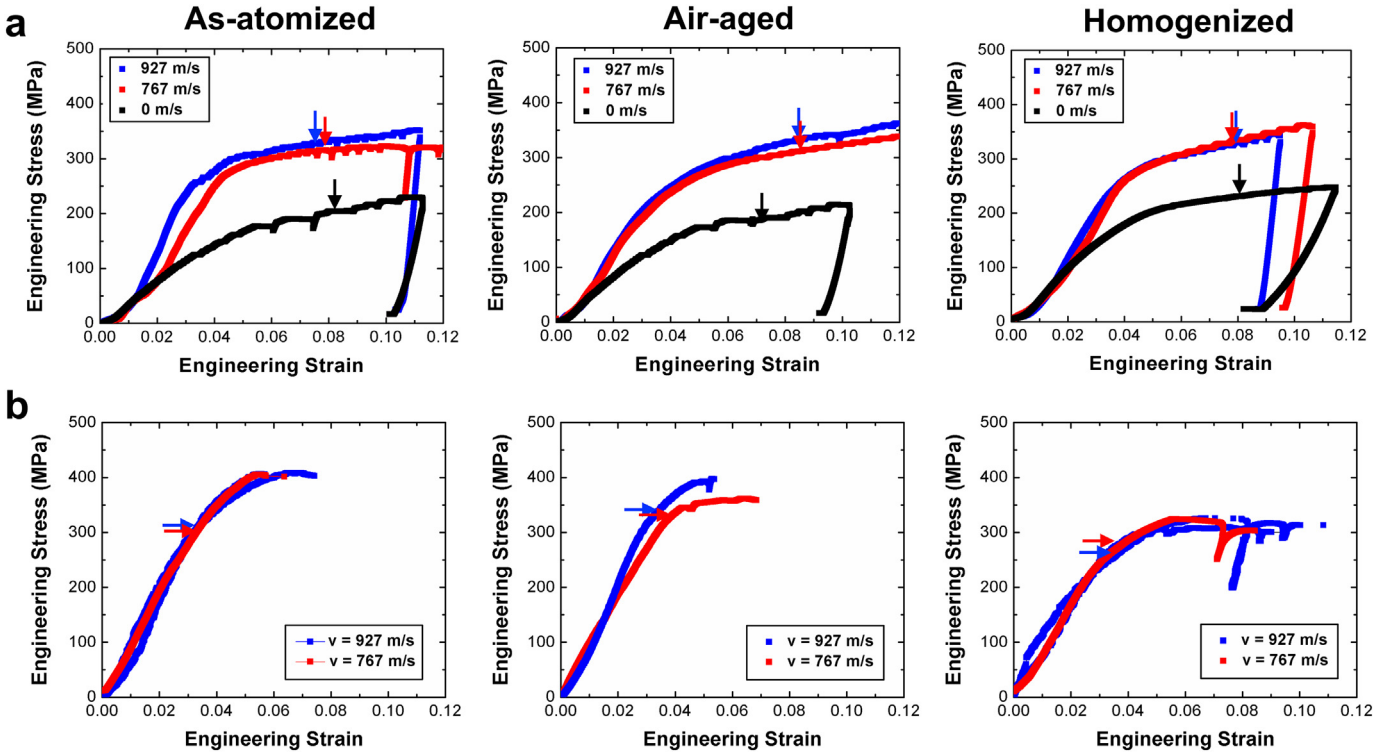

Fig. 2. Representative stress-strain curves from micro-mechanical tests performed in: (a) compression and (b) tension; of the as-atomized, air-aged, and homogenized powder samples. The arrows indicate the flow stress at 0.05 plastic strain for compression results and the flow stress at 0.005 plastic strain for tension. The larger offset strain was used for compression results to accomodate early plastic yielding due to surface roughness.

The substantial increase in flow stress after impact should result from strain hardening caused by the increase in dislocation density. In addition, it is interesting to note that the flow stress for the splats does not exhibit the same variation with heat-treatment condition as that observed for the corresponding powder particles. This is presumably because the high dislocation density in these splats is the dominant factor in determining the flow stress, so that the effects of other microstructural features such as precipitates and solute concentration do not produce measurable differences.

Evidence for such extremely high dislocation densities was obtained in the form of high-angle annular dark-field (HAADF) STEM images from FIB-cut cross-sectional specimens through the splats; examples from the 767 m/s splats of the as-atomized and homogenized powders are presented in Fig. 3. Interestingly, the dislocations do not form any localized entanglement that are often observed in high-strain rate deformed metals. Rather, all of the dislocations seem to be relatively evenly distributed. One can estimate the dislocation density from HAADF STEM images such as Fig. 3 by measuring the average spacing between dislocation segments using the line intercept method (i.e. by counting the number of intersecting points between dislocations on arbitrary straight lines across the images). The values of dislocation spacing are approximately 20–30 nm corresponding to dislocation densities of $1.1–1.6\times10^{15}$ m^{-2}. These values are of the same order of magnitude as the densities of dislocation networks in severely deformed metals [28].

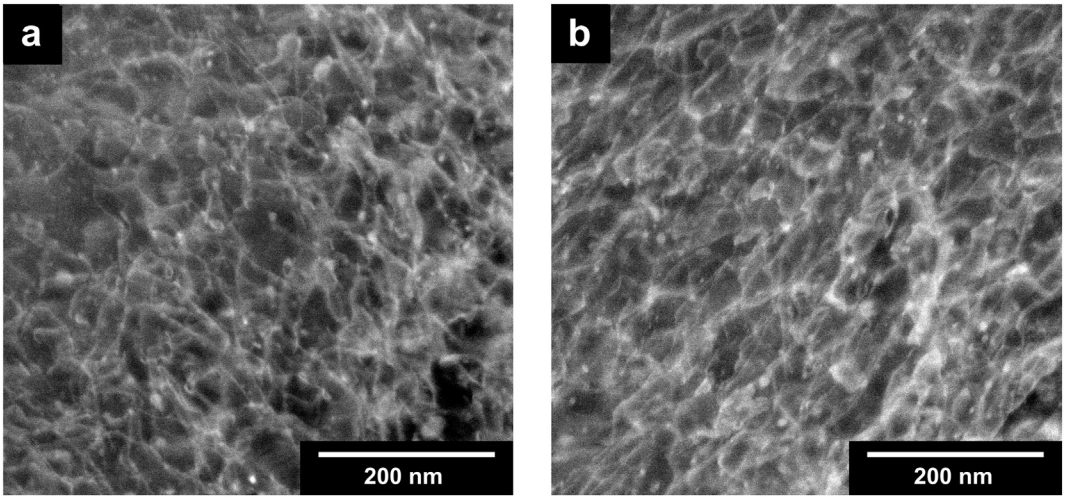

Fig. 3. HAADF STEM images of the dislocation structures in the splats of the (a) as-atomized and (b) homogenized splats. Note that these dense dislocation networks are present uniformly throughout the splats. The average dislocation spacing is around 20–30 nm.

The measured dislocation density can be used to estimate the yield strength expected on the basis of dislocation motion only via the Taylor equation, which gives $\sigma_y \approx 2 \times \tau_y = 2 \times \alpha\mu b\sqrt{\rho} \approx 250 \sim 300\,MPa$, where σ_y is the uniaxial yield strength, τ_y is the shear yield strength, α is the Taylor coefficient (0.5), μ is the shear modulus (26 GPa), b is the magnitude of Burgers vector, and ρ is the dislocation density. The yield strength values from the Taylor equation are similar to the flow stress values measured experimentally in this study. Motion of dislocations in the extremely dense network in the splats would cause plastic yielding before any strong interactions of dislocations with solutes and precipitates occur. The high densities of dislocations seem to dominate the yield behavior of the splats, leading to similar flow stress values regardless of the initial microstructures in the powder.

Similar yield behavior in splats regardless of both initial powder microstructure and impact velocity does not mean that similar yield strength would be obtained in the corresponding bulk cold-spray deposits. The current measurements are obtained from the interior of the powders and splats, and they do not consider the adhesion strength between splats (or between splats and the substrate) and do not contain the most highly worked material near the periphery of the powder particles. The adhesion at the splat-substrate boundary was generally weaker for the 767 m/s splats than for the 927 m/s splats. The tensile tests on 767 m/s splats often showed the interfacial fracture away from the gauge length (see, for example, Supplementary Movie 5), but such effects are not observed for 927 m/s splats. Although both velocities are higher than the critical velocity of adhesion, there seems to be significant variation in adhesion strength depending on the impact velocity.

A key advantage of micro-mechanical tensile testing is that aspects of ductility and fracture behavior are captured. For the current experiments, this was done by comparing video frames just before and after the point of fracture, and by SEM fractography of the failed samples. For the as-atomized samples, little change in the diameter of the sample throughout the test was observed (Fig. 4(a) and Supplementary Movie 2). Failure was abrupt, and clean smooth fracture surfaces were observed, characteristic of brittle failure, presumably near a cell/grain boundary (Fig. 4(b)). For the homogenized samples, however, clear indications of necking during testing were observed, with a localized reduction in the cross-sectional area within the gauge length (Fig. 4 (c) and Supplementary Movie 4). Upon examination of the fracture surface there is clear evidence of necking with the sample coming nearly to a fine point and then tearing (Fig. 4(d)).

The difference in fracture mode can be explained by the variation in the microstructure between the as-atomized or air-aged samples and the homogenized samples. Previous microstructural characterization studies have revealed that the as-atomized and air-aged powder particles comprise several cellular-dendritic grains defined by high-angle grain boundaries, with the individual cells being separated by low-angle grain boundaries [27]. These low-angle grain boundaries are decorated with thin (≈10 nm) films of alternating Mg-rich and Fe-rich secondary phases that inhibit slip transfer and result in brittle boundary failure. After homogenization, there is dissolution of the Mg-rich phase, and coarsening of the Fe-rich phase [27]. As a result, the cell boundaries become less well-defined, allowing the dislocations to move more freely, and leading to more ductile failure.

In summary, this study investigated the effects of supersonic impact on the mechanical response of cold-sprayed Al6061 powders by performing in-situ micropillar compression and tension, and transmission electron microscopy. The following results were observed:

(1) The flow stresses of the splats are not dependent on the impact velocity under the conditions considered here, presumably due to the saturation of dislocation density.
(2) The flow stresses of the splats are not dependent on the initial powder microstructure. Extremely high dislocation density dominates the effects of other microstructural features.
(3) The ductility of the splats is dependent on the initial powder microstructure. Homogenized powder particles give higher ductility splats due to dissolution and coarsening of cell boundary phases, the removal of the cell boundaries allows for slip transfer across the boundaries.

This approach can be used more generally to study other supersonic impacted metallic powder particles. Furthermore, the results will not only give an important fundamental insight into the mechanical behavior of post-supersonic-impacted metallic materials, but will also be very useful to help develop an understanding of the bulk mechanical behavior of cold-spray deposits by providing a microscopic perspective of the cold spray processes.

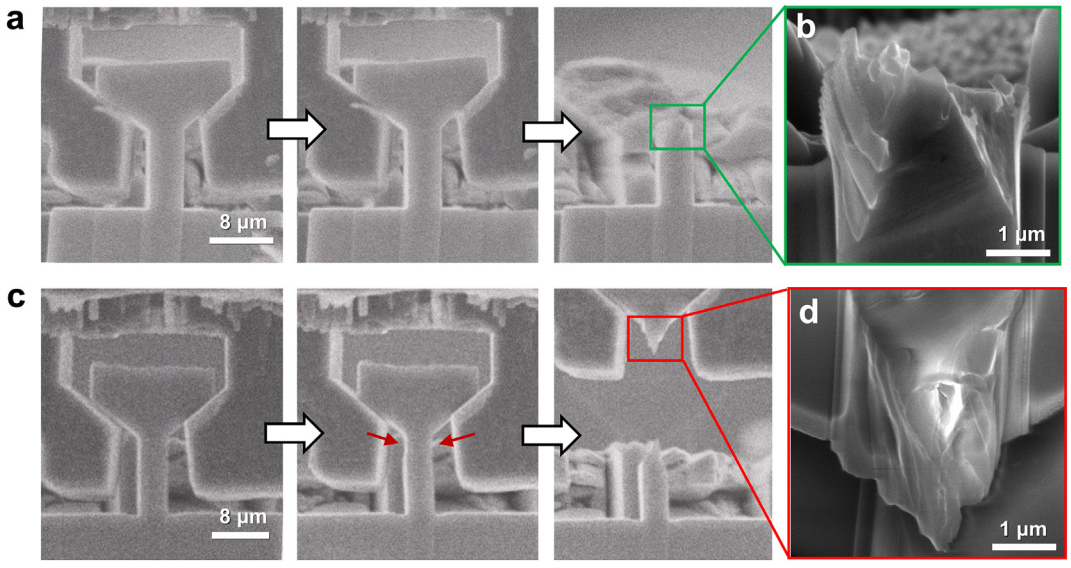

Fig. 4. SEM images showing the fracture mode in micro-mechanical tensile tests on: (a, b) an as-atomized splat; (c, d) an homogenized splat. The tensile deformation of the homogenized splat clearly shows the formation of necking (red arrows).

Supplementary data to this article can be found online at https://doi.org/10.1016/j.scriptamat.2019.06.024.

Acknowledgement

This research was supported by the U.S. Army Research Laboratory under contract W911NF-15-2-0024 titled "Intelligent Processing of Materials by Design." The microscopy studies in this paper were performed using facilities in the UConn/Thermo Fisher Scientific Center of Advanced Microscopy and Materials Analysis (CAMMA).

References

[1] V.K. Champagne, Ed., The Cold Spray Materials Deposition Process: Fundamentals and Applications, Woodhead Publishing Limited, Abington Hall, (2007).
[2] T.H. Van Steenkiste, J.R. Smith, R.E. Teets, J.J. Moleski, D.W. Gorkiewicz, R.P. Tison, D.R. Marantz, K.A. Kowalsky, W.L. Riggs II, P.H. Zajchowski, B. Pilsner, R.C. McCune, K.J. Barnett, Surf. Coat. Technol. 111 (1999) 62–71.
[3] T. Stoltenhoff, H. Kreye, H.J. Richter, J. Thermal Spray Technol. 11 (2002) 542–550.
[4] A. Moridi, S.M. Hassani-Gangaraj, M. Guagliano, M. Dao, Surf. Eng. 36 (6) (2014) 369–395.
[5] S. Suresh, S.-W. Lee, M. Aindow, H. Brody, V.K. Champagne, A.M. Dongare, Sci. Rep. 8 (2018), 10075.
[6] A.C. Hall, L.N. Brewer, T.J. Roemer, J. Thermal Spray Technol. 17 (3) (2008).
[7] R.C. Dykhuizen, M.F. Smith, D.L. Gilmore, R.A. Neiser, X. Jiang, S. Sampath, J. Thermal Spray Technol. 8 (4) (1999) 559–564.
[8] M. Grujicic, C.L. Zhao, W.S. Derosset, D. Helfritch, Mater. Des. 25 (2004) 681–688.
[9] H. Assadi, F. Gärtner, T. Stoltenhoff, H. Kreye, Acta Mater. 51 (2003) 4379–4394.
[10] H. Assadi, H. Kreye, F. Gartner, T. Klassen, Acta Mater. 116 (2016) 382–407.
[11] V.K. Champagne, J. Fail. Anal. Prev. 8 (2008) 164–175.
[12] V.K. Champagne, D. Helfritch, Mater. Sci. Technol. 31 (6) (2015) 627–634.
[13] V. Luzin, K. Spencer, M.-X. Zhang, Acta Mater. 59 (2011) 1259–1270.
[14] P. Cavaliere, A. Silvello, Int. J. Adv. Manuf. Technol. 81 (2015) 1857–1862.
[15] B. Marzbanrad, H. Jahed, E. Toyserkani, Mater. Des. 138 (2018) 90–102.
[16] K. Spencer, D.M. Fabijanic, M.-X. Zhang, Surf. Coat. Technol. 204 (2012) 336–344.
[17] S. Rech, A. Trentin, S. Vezzu, E. Vedelago, J.-G. Legoux, E. Irissou, J. Thermal Spray Technol. 23 (8) (2014) 1237–1250.
[18] C.A. Widener, M.J. Carter, O.C. Ozdemir, R.H. Hrabe, B. Hoiland, T.E. Stamey, V.K. Champagne, T.J. Eden, J. Thermal Spray Technol. 25 (1–2) (2016) 193–201.
[19] V.K. Champagne Jr., D. Kaplowitz, V.K. Champagne III, C. Howe, M.K. West, B. McNally, M. Rokni, Mater. Manuf. Proc. 33 (2) (2018) 130–139.
[20] I. Polmear, D. St. John, J.-F. Nie., and M. Qian, Light Alloys Metallurgy of the Light Metals, 5th ed. Butterworth-Heinemann, Burlington, 2017.
[21] T. Schmidt, H. Assadi, F. Gärtner, H. Richter, T. Stoltenhoff, H. Kreye, T. Klassen, J. Thermal Spray Technol. 18 (5–6) (2009) 794–808.
[22] M.R. Rokni, C.A. Widener, V.K. Champagne, Appl. Surf. Sci. 290 (2014) 482–489.
[23] M.R. Rokni, C.A. Widener, V.K. Champagne, J. Thermal Spray Technol. 23 (3) (2014) 514–524.
[24] M.D. Uchic, D.M. Dimiduk, J.N. Florando, W.D. Nix, Science. 305 (2004) 986.
[25] J.R. Greer, W.C. Oliver, W.D. Nix, Acta Mater. 53 (2005) 1821.
[26] C.A. Volkert, E.T. Lilleodden, Phil. Mag. 86 (2006) 5567.
[27] B.A. Bedard, T.J. Flanagan, A.T. Ernst, A. Nardi, A.M. Dongare, H.D. Brody, V.K. Champagne, S.-W. Lee, M. Aindow, J. Thermal Spray Technol. 27 (8) (2018) 1563–1578.
[28] A. Argon, Strengthening Mechanism in Crystal Plasticity, Oxford University Press Inc, New York, 2007.